Microstructure evaluation of UNS S32205 duplex stainless steel friction stir welds

Avaliação microestrutural de juntas soldadas por atrito com pino não-consumível do aço inoxidável duplex UNS S32205

Tiago F. A. Santos
Doutorando em Engenharia Mecânica
Dema/FEM/UNICAMP.
Laboratório Nacional de Nanotecnologia – LNNano/CNPEM
tfa.santos@gmail.com

Ricardo R. Marinho
M.Sc., Pesquisador do CENPES/Petrobras
reppold@petrobras.com.br

Marcelo T. P. Paes
M.Sc., Pesquisador do CENPES/Petrobras
mtpp@petrobras.com.br

Antonio J. Ramirez
Dr., Pesquisador do Laboratório Nacional de Nanotecnologia – LNNano/CNPEM.
Caixa Postal 6192,
Campinas-SP 13083-970, Brasil.
antonio.ramirez@lnnano.org.br

Abstract

UNS S32205 duplex stainless steel welds were performed by friction stir welding (FSW). Advancing and retreating sides showed distinct characteristics in the welded joint. The advancing side shows the strongest grain refinement which is corroborated by microhardness measurements. The microstructure characterization was carried out by optical, scanning and transmission electron microscopy. The thermomechanically affected zone displays austenite islands deformed in a ferrite matrix. The stir zone (SZ) showed a fine recrystallized microstructure providing an outstanding increase of hardness associated with better corrosion performance. Transmission electron microscopy and corrosion tests have corroborated the absence of intermetallic phases on welded joints.

Keywords: Friction stir welding, duplex stainless steel, microhardness, corrosion.

Resumo

Juntas soldadas por atrito com pino foram obtidas para o aço inoxidável duplex UNS S32205. Os lados de avanço e retrocesso da junta soldada evidenciaram diferentes características microestruturais, o lado de avanço apresentou um maior grau de refinamento de grãos, principal mecanismo de aumento de dureza. A caracterização microestrutural foi realizada através de microscopia ótica, eletrônica de varredura e de transmissão. A zona termomecanicamente afetada apresentou ilhas de austenita deformadas em matriz ferrítica. A zona misturada apresentou uma microestrutura fina completamente recristalizada, permitindo um impressionante aumento de dureza, na junta soldada associado a uma melhoria na resistência à corrosão. Avaliações por microscopia eletrônica de transmissão e ensaios de corrosão corroboraram para a ausência de fases secundárias deletérias na junta soldada.

Palavras-chave: *Soldagem por atrito com pino não-consumível, aços inoxidáveis duplex, microdureza, corrosão.*

1. Introduction

Austenitic-ferritic stainless steel also referred to as duplex stainless steels (DSS) combine many of beneficial properties of ferritic and austenitic steels. The chemical composition of duplex steels is balanced to give approximately equal amounts of ferrite and austenite in solution-annealed condition. They are most often selected for corrosion resistance and have replaced austenitic alloys in many applications where stress corrosion cracking and pitting corrosion are concerns. However, DSS has a limited service temperature range, below 300°C, because a great number of detrimental secondary phases can be formed as a consequence of the thermodynamic instability of the ferrite (Lippold et al., 2005; Lo et al., 2009).

Due to their low nickel content, DSS has good weldability. However, the melting and solidification associated with fusion welding processes can destroy the favorable duplex microstructure of these stainless steels. Moreover, detrimental intermetallic phases can be formed during the fusion welding process. Higher ferrite content and coarser grains are other factors which decrease both corrosion resistance and mechanical properties of the welded joint (Sato et al., 2005; Steel et al., 2004).

Friction stir welding (FSW) is a solid-state joining process, which shows some advantages to welding DSS. For example, fusion welding associated problems are eliminated. FSW has achieved satisfactory products with better mechanical properties for several systems, mainly aluminum alloys, when compared to conventional fusion welding techniques. Nevertheless, some authors have showed good results for DSS (Sato et al., 2005; Saied et al., 2008). During FSW process, the material is submitted to intense plastic deformation at elevated temperature resulting in generation of fine and equi-axed recrystallized grains (Mishra et al., 2007).

2. Experimental procedure

The study was performed on a commercial grade UNS S32205 duplex stainless steel with typical chemical composition indicated in Table 1. The chemical composition was provided by the steel producer, Aperam. A common characteristic of all duplex grades is their high mechanical strength. Their yield strength is about twice that of the most common austenitic grades (yield and tensile strength ~ 450 MPa and 620 MPa, for UNS S32205 DSS, respectively) and is much higher than that of ferritic stainless steels (Paijkull et al., 2008) associated to hardness around 280 HV (0.2/15).

C	Mn	Si	Cr	Ni	Mo	P	S	N
0.023	1.80	0.30	22.5	5.4	2.8	0.030	0.001	0.16

Table 1
Typical chemical composition (wt %) of the of UNS S32205 duplex stainless steel.

Plates of 350 x 150 x 6 mm were friction stir welded normal to the rolling direction. The joints were performed using a dedicated TTI FSW, which allows position and force controlled welding. A downward force of 40 kN (force controlled process) was necessary to produce sound welds using an un-tilted PCBN-40%WRe metal matrix composite tool with threaded conical shape and 6 mm long pin and convex threaded shoulder. Welding speeds were limited to keep the forces in the welding direction (x direction) at or below 15 kN in order to extend the tool life. Final parameters for UNS S32205 steel consisted of 200 rpm and 100 mm.min^{-1}. An argon atmosphere was introduced through a gas cup around the tool at a flow rate of 1.68 m^3.h^{-1}.

Welds and base metal (BM) were sectioned and polished for optical metallography. The metallographic preparation consisted of sanding and polishing with 1-µm grain diamond paste; final polishing was performed in the Vibromet® vibratory polisher with a 0.05-µm silica solution. Electrolytical etching was used in order to reveal the microstructure. The etching solution consisted of 40 %-vol. HNO_3 in distilled water. Voltage and etching time were 1.50 V and 75 s, respectively.

An Olympus microscope with a PAXCam digital camera was used for all optical microscopy performed in this study. PAX-it!® software was used for images capture. The volumetric fraction of BM was measured by PAX-it. Scanning electron microscopy (SEM) analysis was carried out on a JEOL JSM 5900 LV.

Vickers microhardness map was performed through LECO® microindentation hardness testers using a load of 1.96 N (200 gf) for 15 s.

The corrosion resistance was evaluated for base metal and stir zone on the joint c using cyclic polarization test in 3.5% NaCl solution (artificial sea water) according ASTM G8 with a conventional three-electrode cell using Pt foil as the counter electrode and a saturated calomel electrode (SCE) as the reference. The experiments were initiated after the steady state open circuit potential had been established and maintained for about 60 minutes according to general recommendations of the ASTM G61 standard. After that, a potential sweep came through the anodic direction at 1 mV/s until the current density of 1 mA/cm^2 or a potential of 1.2 V was reached.

3. Results and discussion

Preliminary FSW tests were performed in position control mode to determine the best tool penetration that provides sound welds, adequate surface finishing, and reasonable axial and transverse forces. Then, the final welds were performed in force control mode with 200 rpm of spindle speed and 100 mm/min of welding speed. During the welding process the tool achieved a maximum temperature below 850°C. However, this thermocouple positioned by the tool shoulder does not provide the exact tool temperature at the interface with the processing material within the stir zone. Nevertheless, due to the high thermal conductivity of PCBN-40%WRe tool, it provides a comparative value for different welding parameters and

final microstructures (Steel et al., 2004). In fact, previous works have showed a peak temperature on UNS S32205 FSW joints around 1100°C (Santos et al., 2010). Proper tool depth was controlled by Z axis load. The force in the welding direction was kept below 15 kN.

The microstructure of the welded joint can be classified into four distinct regions including the stir zone (SZ), heat affected zone (HAZ), thermomechanically affected zone (TMAZ), and base metal (BM) according to Figure 1. However, The HAZ has not been observed on DSS FSWed joints (Sato et al., 2005) Figure 1 displays macro and microstructures of the cross-section at different regions of the welded joint.

The BM is shown in Figure 1 (B) and its microstructure consists of austenite islands in a ferritic matrix. TMAZ near to the retreating side (RS) is shown in Figure 2(C), where deformed austenite grains were observed. No significant grain growth was observed.

Figure 1 (D) displays the SZ center, where austenite grains appear to be more deformed than the ferrite. In the case of duplex alloys both phases deform differently and recrystallize according to distinct kinetics (Padilha et al., 2005). Although austenite has a higher recrystallization potential, diffusion in ferrite is quicker than in austenite. Thus, ferrite undergoes complete recrystallization and grain growth while austenite shows only partial recrystallization. Some authors (Sato et al., 2005; Saied et al., 2008) have pointed out a larger deformation on FSW, the occurrence of continuous dynamic recrystallization for ferrite, and discontinuous dynamic recrystallization for austenite.

Figure 1 (E) shows the zone with the strongest grain refinement in the advancing side of the welded joint. Steel el al. (2004) and Sato et al (1999) working on FSW of UNS S32750 also reported stronger grain refinement in the advancing side of the SZ. Figure 1F shows the SZ/TMAZ interface.

Figure 2 shows the microstructure of the retreating (A) and advancing (B) sides of the stir zone by scanning electron microscopy (SEM). On the AS, it is possible to observe a stronger grain refinement than on the RS side. However, fully recrystallized grains of both phases can be observed in both zones. The AS achieves the highest deformation level favoring recrystallization. The microstructure on the root of welded joints is shown in Figure 2(C), where a microstructure similar to the SZ is observed, with fine austenite and ferrite grains. The TMAZ on the advancing side is shown in Figure 2(D), where austenite islands appear to be deformed in a ferrite matrix. Deleterious secondary phases were not observed in any region by SEM.

Characterization of the SZ-AS by transmission electron microscopy (TEM) is shown in Figure 3(A). Equiaxed grains with low density of dislocations are observed corroborating the fully recrystallized microstructure. Figure 3(B) and (C) show the indexed diffraction patterns of two austenite grains observed in Figure 3(A). No precipitation was indicated by TEM evaluation.

The hardness map of the welded joint is shown in Figure 4. An overall increase of hardness is observed due to refined microstructure on the SZ. The advancing side indicated the strongest grain refinement level. The hardness increase in the stir zone suggests that it is related to the grain size of ferrite and austenite phases in the welded joint as suggested by Hall-Petch relation. The austenite islands morphology in the stir zone was distinct from that of the base metal. This effect is due to the intense plastic strain to which

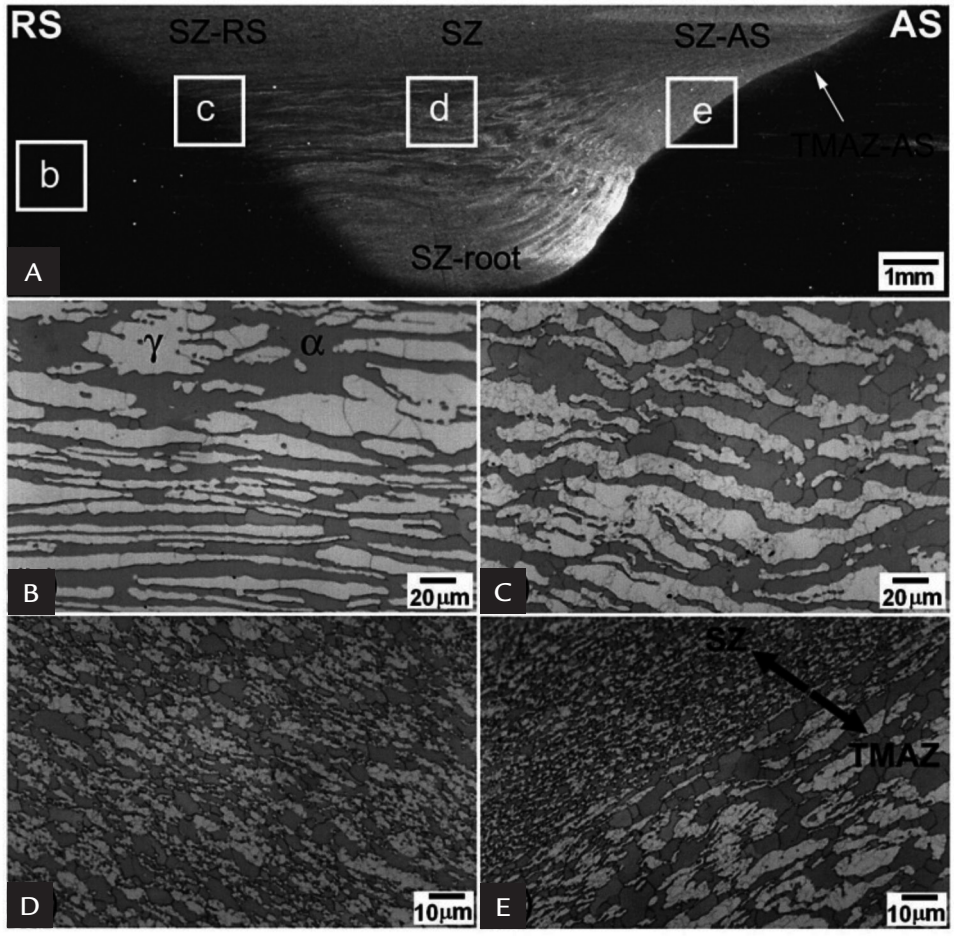

Figure 1
Cross-section of
UNS S32205 DSS FSWed joint
A) macrograph of welded joint.
B) BM.
C) TMAZ-AS.
D) SZ.
E) interface SZ/TMAZ-AS.
Optical microscopy.

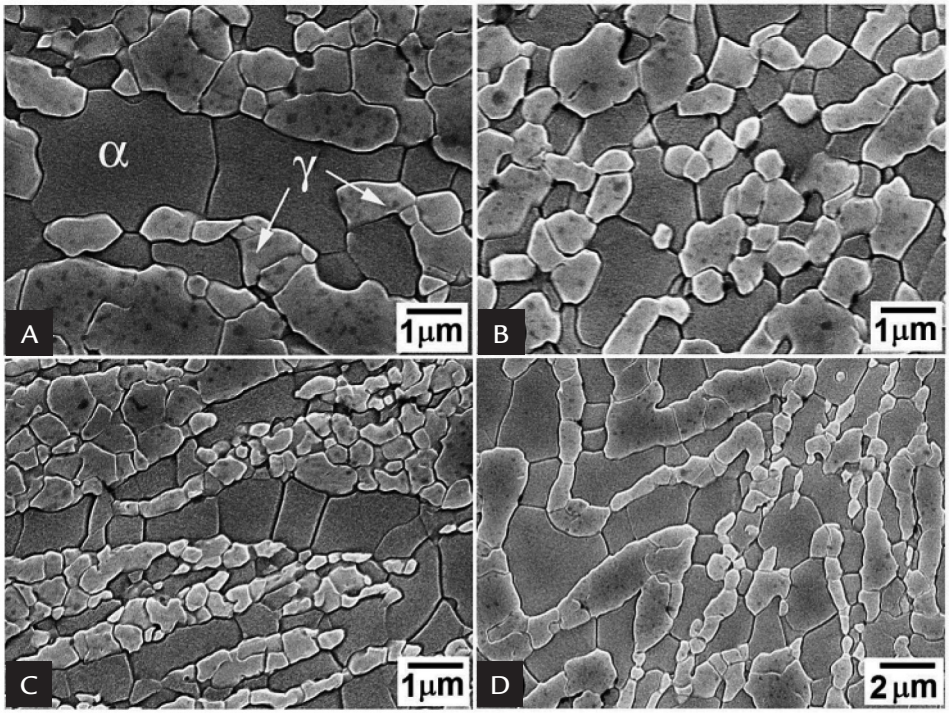

Figure 2
Ferrite (α) and austenite (γ) distributions on the
(A) SZ-RS,
(B) SZ-AS,
(C) SZ-root,
(D) TMAZ-AS. (SEM)

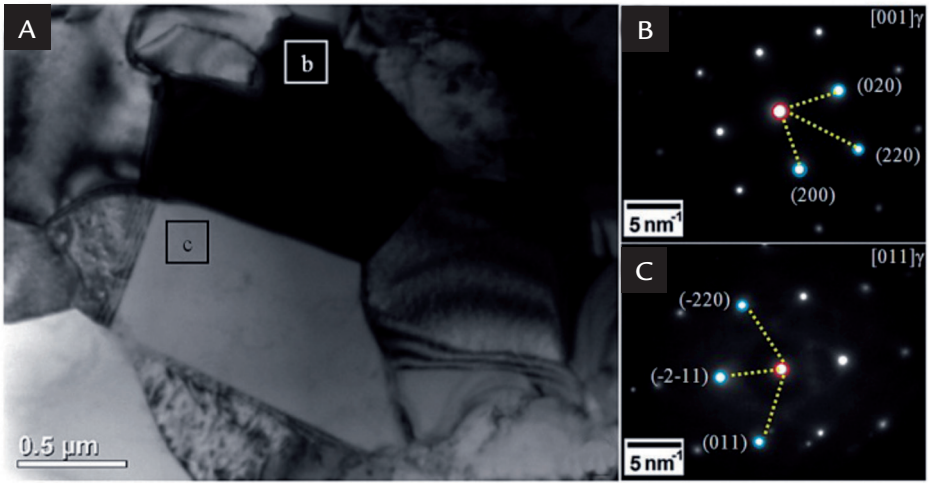

Figure 3
(A) TEM characterization showing the equiaxed fine microstructure in the SZ-AS with (B) and (C) respective indexed diffraction patters.

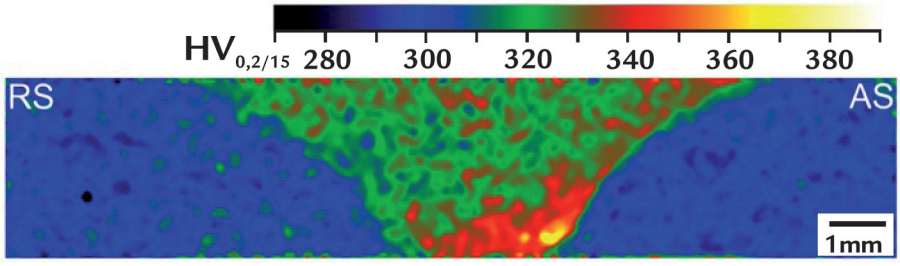

Figure 4
Hardness map showing the overall increase of hardness in the welded joint compared to the base metal.

the austenite was submitted during FSW (Sato et al., 2005; Saied et al., 2008).

The corrosion performance was evaluated by cyclic polarization curves shown in Figure 5. The corrosion potential (Ecorr) and corrosion current density (icorr) were similar in both BM and SZ, around -0.19 V(SCE) and 1.15×10-7 A/cm^2, respectively. Additional information can be extracted from cyclic polarization (CP) curves. CP curves have cathodic and anodic branches, but the anodic branch extends to a wider potential range reaching up to 1.2 V of open circuit potential (OCP) or current density of 1 mA/cm^2, then the potential decreases towards OCP. Additionally to primary passivation potential (Epp) and breakdown potential (Eb), some quantities that help to understand the corrosion behavior are the curve hysteresis and the repassivation potential (Erp). CP curve hysteresis can provide information about corrosion behavior, because positive hysteresis occurs when the damaged passive film is not repaired and/or pitting is initiated. On the other hand, negative hysteresis indicates that the damaged passive film repairs itself (Tait, 1994). CP curves of the BM indicated an initial negative hysteresis behavior with a crossover between the direct and reverse current densities, suggesting the rupture of the passive film, making possible localized corrosion. On the other hand, the SZ CP curves showed a clear negative hysteresis indicating improvements in the corrosion behavior. Additionally, pit growth is not stable on the welded joint because Erp is larger than Ecorr.

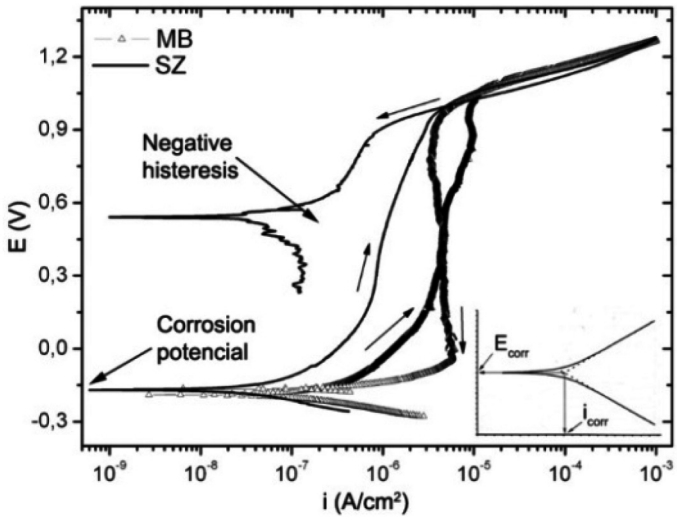

Figure 5
Curves of cyclic polarization indicating the improvement of corrosion resistance in the welded joint.

4. Conclusions

- The present study examined the microstructure, mechanical properties, and corrosion behavior of FSW in UNS S32205 duplex stainless steel using PCBN W-Re tool.
- Complete recrystallized ferrite and austenite grains were observed in the stir zone of the welded joint.
- The thermomecanically affected zone presented deformed austenite islands on a ferrite matrix.
- Secondary phase precipitation was not observed in the welded joint as indicated by the transmission electron microscopy evaluation and corrosion tests.
- Friction stir welding is a very promising joining technology for duplex stainless steels because of the good mechanical and corrosion performance observed in the studied joints. Nevertheless, further research and extensive testing is needed before such technology can be considered for deployment.

5. Acknoledgements

The authors are thankful to Petrobras and FINEP for financial support, to CNPq for scholarships, and to Aperam for material donation.

6. References

ASTM G61-86. Standard test method for conducting cyclic potentiodynamic polarization measurements for localized corrosion susceptibility of iron-, nickel-, or cobalt-based alloys. West Conshohocken, PA: ASTM, 2009.

LIPPOLD, J.C. et al. Welding metallurgy and weldability of stainless steels. In: LIPPOLD, J.C. et al. (eds.). Duplex stainless steels. Ohio: John Wiley & Sons, 2005 , cap. 7, p. 230-263. 357 p.

LO, K.H. et al. Recent developments in stainless steels. ***Mat. Sci. Eng. R***, v. 65, p. 39-104, 2009.

MISHRA, R.S. et al. Friction stir welding and processing. Ohio: ASM International, 2007, 360 p.

PADILHA, A.F. et al. Encruamento, recristalização, crescimento de grão e textura. São Paulo: Associação Brasileira de Metalurgia e Materiais, 2005. 232p.

PAIJKULL, M. et al. The use of duplex stainless steel grades in tubular products. ***Steel Stainless Steel World***, p. 71-79, 2008.

SAEID, T. et al. Effect of friction stir welding speed on the microstructure and mechanical properties of a duplex stainless steel. ***Materials Science and Engineering A***, v. 496, p. 262-268, 2008.

SATO, Y.S. et al. Microstructure and mechanical properties of friction stir welded SAF 2507 super duplex stainless steel. ***Materials Science and Engineering A***, v.397, p.376-384, 2005.

STEEL, R.J. et alii. Friction stir welding of SAF 2507 (UNS S32750) super duplex stainless. ***Steel Stainless Steel World***, v.16, p. 1-16, 2004.

TAIT, S.W. An introduction to eletrochemical corrosion testing for practing engineers and scientists, ***Pair Docs Publications***, 1994.

Paper submitted to INOX 2010- 10th Brazilian Stainless Steel Conference, September 20-22, Rio de Janeiro, Brazil. Revised accepted December, 11, 2012.